JPE 18-6-8

https://doi.org/10.6113/JPE.2018.18.6.1683
ISSN(Print): 1598-2092 / ISSN(Online): 2093-4718

Modeling, Analysis, and Enhanced Control of Modular Multilevel Converters with Asymmetric Arm Impedance for HVDC Applications

Peng Dong*, Jing Lyu*, and Xu Cai†

†,*Wind Power Research Center, School of Electronic Information and Electrical Engineering, Shanghai Jiao Tong University, Shanghai, China

Abstract

Under the conventional control strategy, the asymmetry of arm impedances may result in the poor operating performance of modular multilevel converters (MMCs). For example, fundamental frequency oscillation and double frequency components may occur in the dc and ac sides, respectively; and submodule (SM) capacitor voltages among the arms may not be balanced. This study presents an enhanced control strategy to deal with these problems. A mathematical model of an MMC with asymmetric arm impedance is first established. The causes for the above phenomena are analyzed on the basis of the model. Subsequently, an enhanced current control with five integrated proportional integral resonant regulators is designed to protect the ac and dc terminal behavior of converters from asymmetric arm impedances. Furthermore, an enhanced capacitor voltage control is designed to balance the capacitor voltage among the arms with high efficiency and to decouple the ac side control, dc side control, and capacitor voltage balance control among the arms. The accuracy of the theoretical analysis and the effectiveness of the proposed enhanced control strategy are verified through simulation and experimental results.

Key words: Asymmetric arm impedance, Capacitor voltage balance, Control, Modular multilevel converter (MMC)

I. INTRODUCTION

Modular multilevel converters (MMCs) have become promising converter topologies for high-power applications, such as high-voltage direct current (HVDC) transmission, large motor drives, and many other important future applications, due to their modularity, scalability, and low power losses [1]-[6].

The topology of MMCs was first proposed by Marquardt [7]. The original topology featured no inductors in the arms, and all submodules (SMs) were treated as switchable dc sources. Subsequently, a series inductor was added in each arm to control and limit the arm current [8]. Driven by the complex structure and internal dynamics of MMCs, considerable efforts have been devoted to the development of suitable mathematical models and control strategies. Established MMC models differ from one another in terms of assumptions and simplifications. Ref. [9] proved that MMCs can be analyzed on the basis of the total capacitor voltage rather than the individual capacitor voltage; hence, the model and control are greatly simplified. An average model of an MMC was established by introducing an average operator in a switching cycle [10]; the steady-state analytical expression of circulating currents was obtained, and the coupling effects of capacitance and inductance in the arms were revealed. A decoupled model of ac side, dc side, and circulating currents was established on the basis of the average model under normal conditions [11].

The control strategies available in the literature can be classified into two categories. The first category comprises the direct modulation-based control strategy, which is also known as the non-energy-controlled strategy [12]-[14]. This control strategy is known to be asymptotically stable, but it is prone to large double frequency circulating currents produced by the interaction between modulation signals and SM capacitor voltage ripples. Ref. [15] proposed a circulating

Manuscript received Jul. 6, 2018; accepted Sep. 6, 2018
Recommended for publication by Associate Editor Liqiang Yuan.
†Corresponding Author: xucai@sjtu.edu.cn
Tel: +86-21-34207001, Fax: +86-21-34207470, Shanghai Jiao Tong University
*Wind Power Research Center, School of Electronic Information and Electrical Engineering, Shanghai Jiao Tong University, China

© 2018 KIPE

current suppressi ng control to eliminate double frequency circulating currents. A repetitive controller and a series of resonant controllers were also proposed to solve this problem [16], [17]. The second category comprises the indirect modulation-based control strategy, which is also known as the energy-controlled strategy [18]-[20]. In this case, the balancing of capacitor voltages among different arms is marginally stable, and a closed-loop arm capacitor voltage balancing controller should be employed. These strategies are mainly designed for ideal symmetrical operations. For the studies under asymmetric ac grid conditions, ref. [21], [22] confirmed the existence of positive- and zero-sequence components in circulating currents. A dual vector current control with a supplementary dc voltage ripple suppressing controller was proposed to solve this problem [23]. The control strategy has a relatively complicated structure despite its good performance under asymmetric ac grid conditions. Recently, proportional resonant (PR) controllers have been integrated in circulating current suppressing strategies of MMCs [24], [25]. PR controller-based strategies can completely eliminate all positive-, negative-, and zero- sequence circulating currents in stationary frames. Hence, they can simplify the control structure and improve overall performance.

All the above studies assumed that the arm impedances of MMCs are identical. However, the inductances of the upper and lower arms could inevitably have several differences due to the manufacturing problems in practical projects. In the case of failures, SMs are prone to short-circuit faults, and converters can continue to operate due to redundant configurations. Therefore, the different numbers of failed SMs and different losses in the upper and lower arms cause the arm equivalent resistance to be asymmetric. Ref. [26] briefly introduced the impact of an MMC with asymmetric arm impedance and indicated that the ac current is unequally split between the upper and lower arms. However, neither the influence of the ac current flowing into the dc side caused by asymmetric arm impedance nor the effective control strategy was investigated. Ref. [27] proposed a control strategy for an MMC with asymmetric arm impedance that could eliminate fundamental and double frequency circulating currents and balance arm capacitor voltages. However, the dc current might occur in the ac side of the converter under equivalent resistance conditions of asymmetric arms. Such condition adversely affects transformer operation and ac side performance.

The present study establishes a mathematical model for an MMC with asymmetric arm impedance and analyzes the causes of abnormal phenomena. On the basis of this model, an enhanced current control with five integrated proportional integral resonant (PIR) regulators is designed in an $\alpha\beta 0$ reference frame for MMCs with asymmetric arm impedance in HVDC transmission systems to eliminate the fundamental frequency oscillations in the dc side and the dc and double frequency components in the ac side. Furthermore, an enhanced capacitor voltage control is designed to balance the capacitor voltages among the arms with high efficiency and to decouple the ac side control, dc side control, and capacitor voltage balance control among the arms. With the proposed enhanced control strategy, MMCs with asymmetric arm impedance for HVDC applications can realize steady-state and dynamic performance.

The rest of this paper is organized as follows. Section II establishes a mathematical model of an MMC with asymmetric arm impedance and analyzes the causes of abnormal phenomena. Section III describes the enhanced control strategy. Sections IV and V present the simulation and experimental results to verify the effectiveness of the proposed control strategy, respectively. Section VI concludes the paper.

II. Mathematical Model of an MMC with Asymmetric Arm Impedance

Fig. 1 shows the topology of a three-phase MMC. Each leg of the MMC consists of one upper arm and one lower arm connected in series between the dc terminals. Each arm contains cascaded SMs and an arm inductor.

Fig. 2 depicts the average model of the MMC, where L_{ij} and R_{ij} are the arm inductance and equivalent series resistance, respectively. All capacitor voltages in one arm are maintained in a close range by using a balancing algorithm included in the MMC control system [15]. The cascaded SMs of each arm can be equivalent to the controllable voltage source. The positive arm currents are defined as the charging capacitors of the SMs.

The upper and lower arm currents of the MMC can be expressed as

$$\begin{cases} i_{pj} = i_{comj} + \dfrac{i_j}{2} = \dfrac{i_{dc}}{3} + i_{cirj} + \dfrac{i_j}{2} \\ i_{nj} = i_{comj} - \dfrac{i_j}{2} = \dfrac{i_{dc}}{3} + i_{cirj} - \dfrac{i_j}{2} \end{cases} (j = a,b,c) \tag{1}$$

where i_{pj} (i_{nj}) is the upper (lower) arm current; i_{comj}, i_j, and i_{dc} are the common-mode current, ac side, and dc side, respectively; and i_{cirj} is the circulating current, which includes dc and ac components.

According to Kirchhoff's voltage law, the following equations can be derived from Fig. 2:

$$\begin{cases} u_{pj} = u_{\mathrm{dc}} + u_{cirj} - u_j = \dfrac{V_{dc}}{2} - L_{pj}\dfrac{\mathrm{d}i_{pj}}{\mathrm{d}t} - R_{pj}i_{pj} \\ \qquad\qquad - L_T\dfrac{\mathrm{d}i_j}{\mathrm{d}t} - R_T i_j - v_j - u_{no} \\ u_{nj} = u_{\mathrm{dc}} + u_{cirj} + u_j = \dfrac{V_{dc}}{2} - L_{nj}\dfrac{\mathrm{d}i_{nj}}{\mathrm{d}t} - R_{nj}i_{nj} \\ \qquad\qquad + L_T\dfrac{\mathrm{d}i_j}{\mathrm{d}t} + R_T i_j + v_j + u_{no} \end{cases} \tag{2}$$

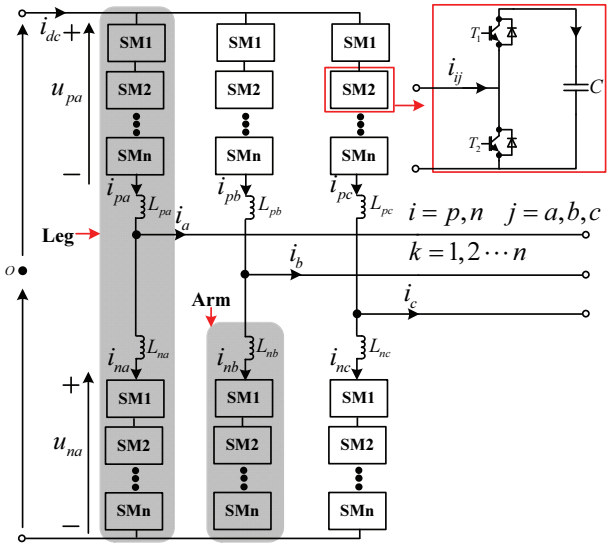

Fig. 1. Topology of the three-phase MMC.

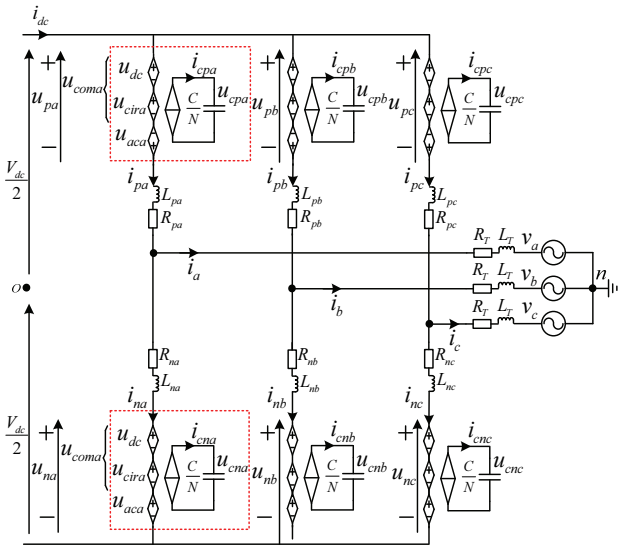

Fig. 2. Average model of MMC.

where u_{pj} (u_{nj}) is the upper (lower) arm voltage; L_{pj} (L_{nj}) is the upper (lower) arm inductance; R_{pj} (R_{nj}) is the upper (lower) arm equivalent resistance; L_T and R_T are the leakage inductance and equivalent resistance of the transformer, respectively; V_{dc} is the dc link voltage; v_j is the ac side voltage; u_j is the ac electromotive force (EMF) (driving i_j); u_{dc} is the dc EMF (driving i_{dc}); u_{cirj} is the internal circulating voltage (driving i_{cirj}); and u_{no} is the common-mode voltage, which is considered to be 0 in this study.

A. Current Model of MMC with Asymmetric Arm Impedance

Combining (1) and (2) yields

$$L_{cj}\frac{di_{comj}}{dt} + R_{cj}i_{comj} = V_{dc} - 2u_{dc} - 2u_{cirj} - \frac{L_{dj}}{2}\frac{di_j}{dt} - \frac{R_{dj}}{2}i_j \tag{3}$$

$$\frac{L_{cj}}{4}\frac{di_j}{dt} + \frac{R_{cj}}{4}i_j = u_j - v_j - \frac{L_{dj}}{2}\frac{di_{comj}}{dt} - \frac{R_{dj}}{2}i_{comj} - L_T\frac{\mathrm{d}i_j}{\mathrm{d}t} - R_T i_j \tag{4}$$

where

$$L_{cj} = L_{pj} + L_{nj}, \quad L_{dj} = L_{pj} - L_{nj}$$
$$R_{cj} = R_{pj} + R_{nj}, \quad R_{dj} = R_{pj} - R_{nj}$$

Equation (3) describes the common-mode current dynamics of the MMC with asymmetric arm impedance, and Equation (4) describes the ac side dynamics. On the basis of (3) and (4), the models of the common-mode and ac side currents can be obtained, as depicted in Figs. 3(a) and 3(b), respectively. The part in the dashed box in Figs. 3(a) and 3(b) is 0 when the arm impedances are identical, that is, $L_{dj} = 0$, $R_{dj} = 0$. Therefore, the common-mode current and ac side current are decoupled, and good control performance can be achieved by

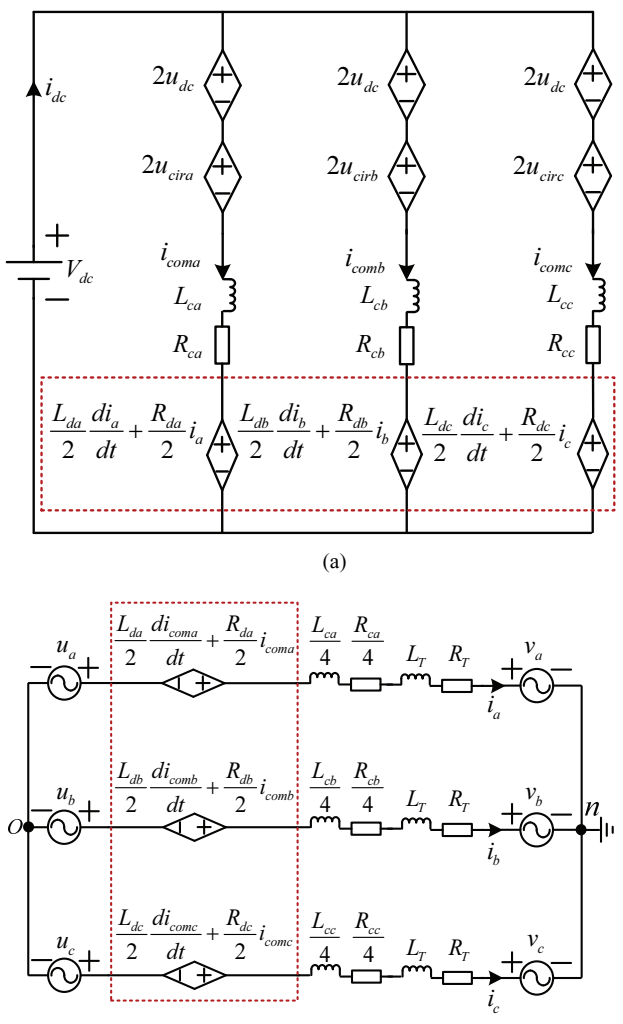

(a)

(b)

Fig. 3. Current model of MMC with asymmetric arm impedance. Cascaded SMs of the upper and lower arms: (a) Common-mode current model; (b) AC side model.

using the conventional current control strategy [15]. However, the part in the dashed box in Figs. 3(a) and 3(b) is not 0 when the arm impedances are asymmetric, that is, $L_{dj} \neq 0$, $R_{dj} \neq 0$. Therefore, ij introduces the fundamental frequency component into icomj when the conventional current control strategy is adopted, as shown in Fig. 3(a). Moreover, fundamental frequency oscillation occurs in the dc side due to the randomness of the arm impedance differences. Similarly, from Fig. 3(b), i_{comj} introduces the dc and double frequency components into i_j. The arm impedances may trigger the transformer protection or overcurrent protection of the fundamental frequency current in the dc line when they are seriously asymmetric. The converter is shut down due to these protection actions.

B. Energy Model of MMC with Asymmetric Arm Impedance

By combining (1) and (2), we can express the instantaneous power of cascaded SMs in the upper and lower arms as

$$\frac{dw_{pj}}{dt} = (u_{comj} - u_j)(\frac{i_{dc}}{3} + i_{cirj} + \frac{i_j}{2}) \tag{5}$$

$$\frac{dw_{nj}}{dt} = (u_{comj} + u_j)(\frac{i_{dc}}{3} + i_{cirj} - \frac{i_j}{2}) \tag{6}$$

where w_{pj} (w_{nj}) is the energy stored in the cascaded SMs of the upper (lower) arm and $u_{comj} = u_{dc} + u_{cirj}$.

The subtraction of (6) from (5) and the addition of (5) and (6) yield

$$\frac{dw_j^{\Delta}}{dt} = -2u_j i_{cirj} + u_{comj} i_j - \frac{2}{3} u_j i_{dc} \tag{7}$$

$$\frac{dw_j^{\Sigma}}{dt} = \frac{2}{3} u_{comj} i_{dc} + 2u_{comj} i_{cirj} - u_j i_j \tag{8}$$

where w_j^{Δ} (w_j^{Σ}) is the difference (sum) of the stored energies.

The dc flows into the ac side, and the fundamental frequency current flows into the dc side under asymmetric arm impedance. Such condition causes the changes in the energy stored in cascaded SMs. By integrating (7) and (8) in a certain fundamental frequency cycle, we have

$$w_j^{\Delta} = \int_t^{t+T} -2u_j i_{cirj} + u_{comj} i_j - \frac{2}{3} u_j i_{dc} dt \neq 0 \tag{9}$$

$$w_j^{\Sigma} = \int_t^{t+T} \frac{2}{3} u_{comj} i_{dc} + 2u_{comj} i_{cirj} - u_j i_j dt \neq w_j^{\Sigma 0} \tag{10}$$

where $w_j^{\Sigma 0}$ is the sum of the energies stored in the cascaded SMs of the upper and lower arms at time "t" and T is a fundamental frequency cycle.

On the basis of (9) and (10), the capacitor voltage imbalance occurs among the different arms under asymmetric arm impedance. The MMC can enter a new steady state when the arm impedances are not seriously asymmetric. However, the capacitor voltage imbalance could lead to different voltage stresses on the switching devices, which will compromise safe operations.

III. Enhanced Control of MMC with Asymmetric Arm Impedance

Eliminating the occurrence of abnormal phenomena in the MMC with asymmetric arm impedance requires the realization of the following control objectives: (1) to eliminate the dc and double frequency components in the ac side, (2) to eliminate the fundamental frequency component in the dc side, (3) to balance the capacitor voltages between the upper and lower arms, and (4) to balance the capacitor voltages among the different legs.

A. Enhanced Current Control Strategy of MMC with Asymmetric Arm Impedance

Achieving the above current control objectives necessitates the direct control of the ac side, dc side, and circulating current by a PIR regulator-based control strategy with high bandwidth. Fig. 4 depicts the block diagram of the enhanced current control strategy with five integrated PIR regulators for the MMC with asymmetric arm impedance. This strategy is designed in the $\alpha\beta 0$ reference frame on the basis of current models.

The asymmetry of arm impedances may lead to the occurrence of dc and double frequency components in the ac side i_α and i_β. To eliminate the dc and double frequency components, we adopt the PIR regulator, the transfer function of which is shown in Equation (11), in tracking the fundamental frequency ac reference signals without steady-state errors, as shown in Fig. 4(a). This approach is in contrast to the conventional current control strategy. The PIR regulator is also used to track the dc reference signals without steady-state errors to eliminate the fundamental frequency oscillations in the dc side i_{dc}. As shown in Fig. 4(c), circulating currents $i_{cir\alpha}$ and $i_{cir\beta}$ can be controlled by using internal circulating voltages $u_{cir\alpha}$ and $u_{cir\beta}$, respectively. The PIR regulator is also adopted to track the dc and fundamental frequency components of the reference signals of the circulating current, as shown in Equation (18). Fig. 4(d) depicts the insertion index generation of each arm, and the arm reference voltages can be linearly obtained by transforming the outputs of the ac side loops, dc side loop, and circulating current loops through matrix A; the expression is presented in the Appendix. The insertion index of each arm, which compensates for capacitor voltage ripples, can be generated by dividing the arm reference voltage by the total capacitor voltage of the corresponding arm.

$$PIR(s) = k_p + \frac{k_i}{s} + \sum_{h=1}^{2} \frac{k_{rh} s}{s^2 + (h\omega_1)^2} \tag{11}$$

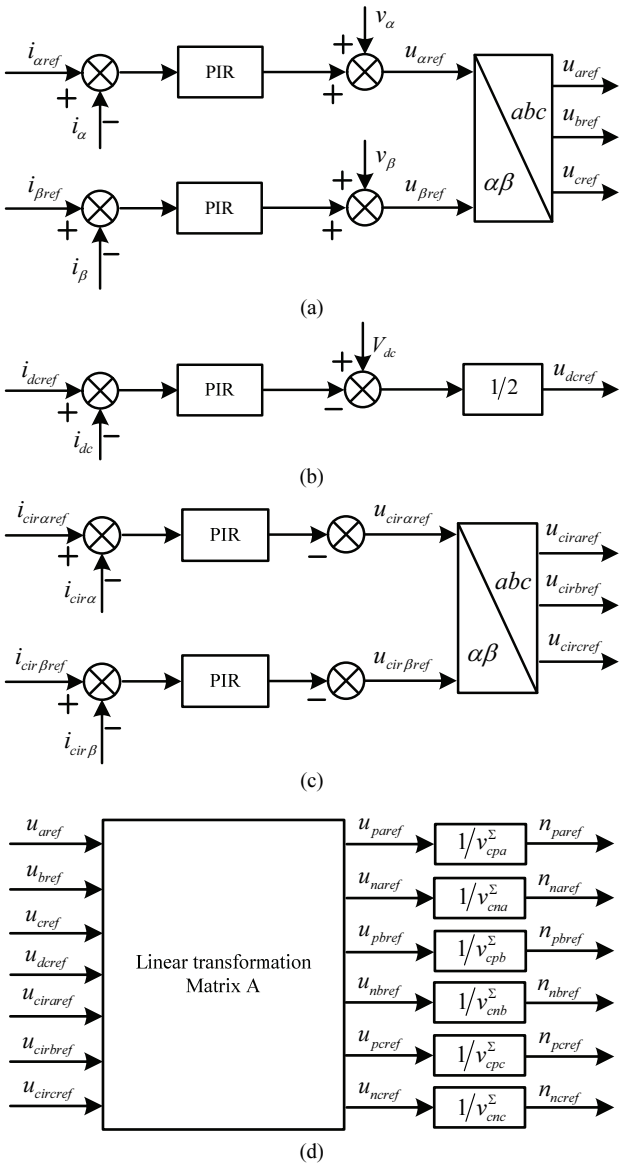

Fig. 4. Enhanced current control strategy of the MMC with asymmetric arm impedance. (a) AC side control; (b) DC side control; (c) Circulating current control; (d) Insertion index generation of each arm.

where k_p, k_i, and k_{rh} are the control parameters of the PIR regulator, and ω_1 is the fundamental angular frequency.

B. Parameter Design of PIR Regulator

As shown in Fig. 3, the dynamics of the ac side, dc side, and circulating current can all be described as first-order systems, which can be expressed as follows:

$$G_{I\{ac,dc,cir\}}(s)=\frac{1}{sL_{\{ac,dc,cir\}}+R_{\{ac,dc,cir\}}} \tag{12}$$

where $L_{\{ac,dc,cir\}}$ are the ac side, dc side, and internal equivalent inductance, respectively; $R_{\{ac,dc,cir\}}$ are the ac side, dc side, and internal equivalent resistance, respectively.

The control parameters of the PIR regulator can be separately tuned [28]. To track the dc reference component without steady-state errors, we use a pure PI regulator for the moment, that is, k_{rh} = 0. The transfer function of the open-loop system can then be derived as

$$G_{K\{ac,dc,cir\}}(s)=\frac{1}{sL_{\{ac,dc,cir\}}+R_{\{ac,dc,cir\}}}\frac{k_p s+k_i}{s} \tag{13}$$

On the basis of the internal mode control approach [29], k_p and k_i can be derived as follows:

$$\begin{cases} k_p=\alpha_c L_{\{ac,dc,cir\}}=\alpha_c\{L_T+\dfrac{L}{2},\dfrac{2L}{3},L\} \\ k_i=\alpha_c R_{\{ac,dc,cir\}}=\alpha_c\{R_T+\dfrac{R}{2},\dfrac{2R}{3},R\} \end{cases} \tag{14}$$

where L and R are the nominal arm inductance and resistance, respectively; and α_c is the desired closed-loop system bandwidth.

By combining (13) and (14), we can express the transfer function of the closed-loop system as

$$G_{C\{ac,dc,cir\}}(s)=\frac{\alpha_c}{(s+\alpha_c)} \tag{15}$$

An upper limit for αc must be ensured for the closed-loop system to remain stable with large margins. A valuable rule of thumb is expressed as follows [30]:

$$\alpha_c\le\frac{\omega_s}{10} \tag{16}$$

where ω_s is the angular sampling frequency.

The recommendation given in (16) typically yields an α_c in the range of kiloradians per second. For example, a sampling frequency of 10 kHz gives $\alpha_c \le 6.3$ krad/s.

To track the ac reference component without steady-state errors, we use a pure PR regulator for the moment, that is, k_i = 0. For simplicity, the equivalent resistance is ignored in designing resonant parameter k_h. Suppose that k_h can be expressed as

$$k_h=\alpha_h k_p \tag{17}$$

By combining (11), (12), (14), and (17), we can derive the transfer function of the closed-loop system as

$$G_{C\{ac,dc,cir\}}(s)=\frac{\alpha_c[s^2+(h\omega_1)^2]+\alpha_h\alpha_c s}{(s+\alpha_c)[s^2+(h\omega_1)^2]+\alpha_h\alpha_c s} \tag{18}$$

This equation can be equivalently expressed as

$$G_{C\{ac,dc,cir\}}(s)=\frac{\alpha_c[s^2+\alpha_h s+(h\omega_1)^2]}{(s+\alpha_c)[s^2+\alpha_h s+(h\omega_1)^2]-\alpha_h s^2} \tag{19}$$

Equation (19) can be approximated as

$$G_{C\{ac,dc,cir\}}(s) \approx \frac{\alpha_c[s^2+\alpha_h s+(h\omega_1)^2]}{(s+\alpha_c)[s^2+\alpha_h s+(h\omega_1)^2]} = \frac{\alpha_c}{(s+\alpha_c)} \quad (20)$$

Equation (20) is simplified as the closed-loop transfer function shown in (15), which is obtained for pure PI control. The approximation holds when

$$\alpha_h \ll \alpha_c \quad (21)$$

This condition translates to a selection of α_h in the range of hundreds of radians per second such that

$$\alpha_h \le \frac{\alpha_c}{10} \quad (22)$$

When k_h is selected on the basis of (16)–(17) and (22), the closed-loop system dynamics will be dominated by a pole at

$$s \approx -\alpha_c \quad (23)$$

In addition, a pole pair is obtained at

$$s \approx -\frac{\alpha_h}{2} \pm j\sqrt{(h\omega_1)^2 - \frac{\alpha_h^2}{4}} \quad (24)$$

However, this pole pair tends to be canceled by the zero pair of G_C(s) in (19), and parameter α_h, which is called the resonant bandwidth, determines the exponential convergence rate of the adjustment made by the *R* part to obtain accurate reference tracking.

C. Enhanced Capacitor Voltage Control Strategy of MMC with Asymmetric Arm Impedance

The capacitor voltage balance is controlled in two stages. The first stage equally distributes the capacitor voltages in each arm, and the second stage balances the capacitor voltages among the different arms. Several techniques have been proposed to balance the capacitor voltages in each arm. They can be classified into distributed and centralized methods [15], [31]-[34]. The distributed method with a closed-loop controller for each SM is effective and is adopted in the present study [15]. In this section, we focus on the design of the enhanced capacitor voltage balance control among different arms.

Only the non-alternating power is considered because the control is focused on regulating the mean value of energy. By transforming (7) to the *αβ0* reference frame, we can derive the dynamics of the differences of the energies stored in the cascaded SMs of the upper and lower arms from the following algebraic calculation:

$$\begin{cases} \dfrac{d\overline{w}_\alpha^\Delta}{dt} = -(v_\alpha i_{cir\alpha}^{ac-} - v_\beta i_{cir\beta}^{ac-}) = e_{dif\alpha} \\ \dfrac{d\overline{w}_\beta^\Delta}{dt} = (v_\alpha i_{cir\beta}^{ac-} + v_\beta i_{cir\alpha}^{ac-}) = e_{dif\beta} \\ \dfrac{d\overline{w}_0^\Delta}{dt} = -(v_\alpha i_{cir\alpha}^{ac+} + v_\beta i_{cir\beta}^{ac+}) = e_{dif0} \end{cases} \quad (25)$$

where $\overline{w}_\alpha^\Delta$, $\overline{w}_\beta^\Delta$, and $\overline{w}_0^\Delta$ are the mean values of the differences of the energies stored in the cascaded SMs of the upper and lower arms in the *αβ0* reference frame; v_α and v_β are the ac side voltages in the *αβ* reference frame; $i_{cir\alpha\beta}^{ac+}$ and $i_{cir\alpha\beta}^{ac-}$ are the positive and negative sequence fundamental frequency ac components of the circulating currents in the *αβ* reference frame, respectively; and $e_{difα}$, $e_{difβ}$, and e_{dif0} are defined as the auxiliary control inputs.

On the basis of (25), the positive and negative sequence fundamental frequency ac components of circulating currents $i_{cir\alpha}^{ac+}$, $i_{cir\beta}^{ac+}$, $i_{cir\alpha}^{ac-}$, and $i_{cir\beta}^{ac-}$ can be used to balance the capacitor voltages between the upper and lower arms. By defining auxiliary control inputs $e_{difα}$, $e_{difβ}$, and e_{dif0}, a PI-based feedback control loop can be designed to regulate the differences of the energies stored in the cascaded SMs of the upper and lower arms by using the resulting first-order system, as shown in Equation (25). However, three types of energy should be controlled, and four ac components of the circulating current should be selected. Therefore, a constraint condition in which the reactive power interaction between the positive sequence fundamental frequency circulating current and the ac side voltage is zero should be added to ensure that the converter achieves the highest efficiency, that is,

$$\frac{3}{2}(-v_\alpha i_{cir\beta}^{ac+} + v_\beta i_{cir\alpha}^{ac+}) = 0 \quad (26)$$

By combining (25) and (26), the reference values of the positive and negative fundamental frequency circulating currents can be expressed as

$$\begin{bmatrix} i_{cir\alpha ref}^{ac+} \\ i_{cir\beta ref}^{ac+} \\ i_{cir\alpha ref}^{ac-} \\ i_{cir\beta ref}^{ac-} \end{bmatrix} = \frac{1}{v_\alpha^2 + v_\beta^2} \begin{bmatrix} 0 & 0 & -v_\alpha & v_\beta \\ 0 & 0 & -v_\beta & -v_\alpha \\ -v_\alpha & v_\beta & 0 & 0 \\ v_\beta & v_\alpha & 0 & 0 \end{bmatrix} \begin{bmatrix} e_{dif\alpha} \\ e_{dif\beta} \\ e_{dif0} \\ 0 \end{bmatrix} \quad (27)$$

By transforming (8) to the *αβ0* reference frame, we can derive the dynamics of the sum of the energies stored in the cascaded SMs of the upper and lower arms from the following algebraic calculation:

$$\begin{cases} \dfrac{d\overline{w}_\alpha^\Sigma}{dt} = 2u_{dc} i_{cir\alpha}^{dc} - \dfrac{1}{2}(v_\alpha i_\alpha^- - v_\beta i_\beta^-) = e_{sum\alpha} \\ \dfrac{d\overline{w}_\beta^\Sigma}{dt} = 2u_{dc} i_{cir\beta}^{dc} + \dfrac{1}{2}(v_\alpha i_\beta^- + v_\beta i_\alpha^-) = e_{sum\beta} \\ 3\dfrac{d\overline{w}_0^\Sigma}{dt} = 2u_{dc} i_{dc} - \dfrac{3}{2}(v_\alpha i_\alpha^+ + v_\beta i_\beta^+) = e_{sum0} \end{cases} \quad (28)$$

where $\overline{w}_\alpha^\Sigma$, $\overline{w}_\beta^\Sigma$, and $\overline{w}_0^\Sigma$ are the mean values of the sum of the energies stored in the cascaded SMs of the upper and

lower arms in the *αβ0* reference frame; $i_{\alpha\beta}^{+}$ and $i_{\alpha\beta}^{-}$ are the positive and negative sequence ac side currents in the *αβ0* reference frame, respectively; $i_{cir\alpha\beta}^{dc}$ is the dc component of the circulating current in the *αβ0* reference frame; and $e_{sum\alpha}$, $e_{sum\beta}$, and e_{sum0} are defined as the auxiliary control inputs.

On the basis of (28), the dc components of circulating currents $i_{cir\alpha}^{dc}$ and $i_{cir\beta}^{dc}$ can be selected to balance the capa citor voltages among different legs because the negative sequence ac side is commonly controlled to zero in HVDC applications. The total energy stored in the capacitors of the converter can be regulated by dc side i_{dc}. The non-alternating power disturbances can be compensated for in a feed-forward manner by defining auxiliary control inputs $e_{sum\alpha}$, $e_{sum\beta}$, and e_{sum0}. Through the control input transformation, a PI-based feedback control loop can be designed to regulate the sum of the energies stored in cascaded SMs by using the resulting first-order system, as shown in Equation (28). The reference of the dc side and the dc components of the circulating current can be expressed as

$$i_{dc}^{ref} = \frac{e_{sum0} + \frac{3}{2}(v_\alpha i_\alpha + v_\beta i_\beta)}{2u_{dc}} \tag{29}$$

$$\begin{cases} i_{cir\alpha ref}^{dc} = \dfrac{e_{sum\alpha}}{2u_{dc}} \\ i_{cir\beta ref}^{dc} = \dfrac{e_{sum\beta}}{2u_{dc}} \end{cases} \tag{30}$$

On the basis of (25)-(30), the block diagram of the enhanced capacitor voltage control strategy of the MMC with asymmetric arm impedance is depicted in Fig. 5. As shown in Fig. 5(a), the reference value of the difference of the energies stored in the cascaded SMs of the upper and lower arms is zero, and the feedback value contains a large fundamental frequency ripple. A 50 Hz notch filter is added in the feedback link to eliminate the influence of the fundamental frequency component. The outputs of three PI regulators are $e_{dif\alpha}$, $e_{dif\beta}$, and e_{dif0}, respectively, and the reference value of the positive and negative fundamental frequency ac components of the circulating current can be obtained on the basis of (27). As shown in Fig. 5(b), a 50 Hz notch filter is added in the feedback link to eliminate the influence of the fundamental frequency component of the feedback value. The output of the PI regulator is e_{sum0}, and the reference value of the dc side can be obtained on the basis of (29). As shown in Fig. 5(c), the reference value of the sum of the energies stored in the cascaded SMs of the upper and lower arms is zero, and the feedback value contains a large double frequency ripple. A 100 Hz notch filter is added in the feedback link to eliminate the influence of the double frequency component. The outputs of two PI regulators are $e_{sum\alpha}$ and $e_{sum\beta}$, respectively, and the

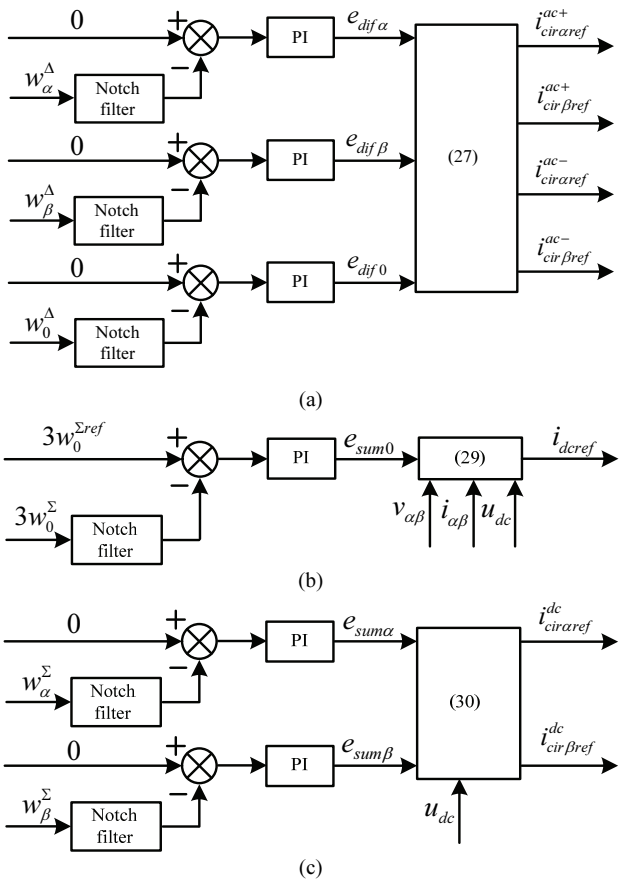

Fig. 5. Enhanced capacitor voltage control strategy of the MMC with asymmetric arm impedance: (a) Capacitor voltage balance control between the upper and lower arms; (b) Total capacitor voltage control; (c) Capacitor voltage balance control among the legs.

reference value of the dc component of the circulating current can be obtained on the basis of (30). Hence, the reference value of the circulating current as the input of the circulating current control shown in Fig. 4(c) can be obtained as

$$\begin{cases} i_{cir\alpha ref} = i_{cir\alpha ref}^{dc} + i_{cir\alpha ref}^{ac+} + i_{cir\alpha ref}^{ac-} \\ i_{cir\beta ref} = i_{cir\beta ref}^{dc} + i_{cir\beta ref}^{ac+} + i_{cir\beta ref}^{ac-} \end{cases} \tag{31}$$

On the basis of Figs. 4(a), 4(b), 5(a), and 5(c), the ac side control, dc side control, and capacitor voltage balance control among the arms are decoupled. Therefore, the MMC with asymmetric arm impedance for HVDC applications can achieve a steady-state and dynamic performance by using the proposed enhanced control strategy.

IV. Simulation Verification

To verify the effectiveness of the proposed enhanced control strategy of the MMC with asymmetric arm impedance for HVDC applications, we build a nonlinear time domain simulation model of the MMC-HVDC system (Fig. 6) in MATLAB/Simulink. MMC1 adopts a fixed active power

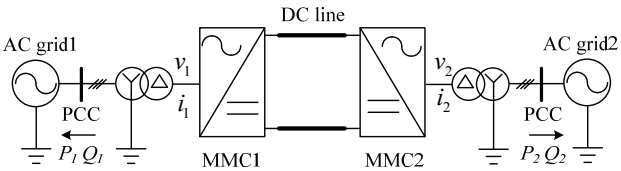

Fig. 6. Structure diagram of the simulation system.

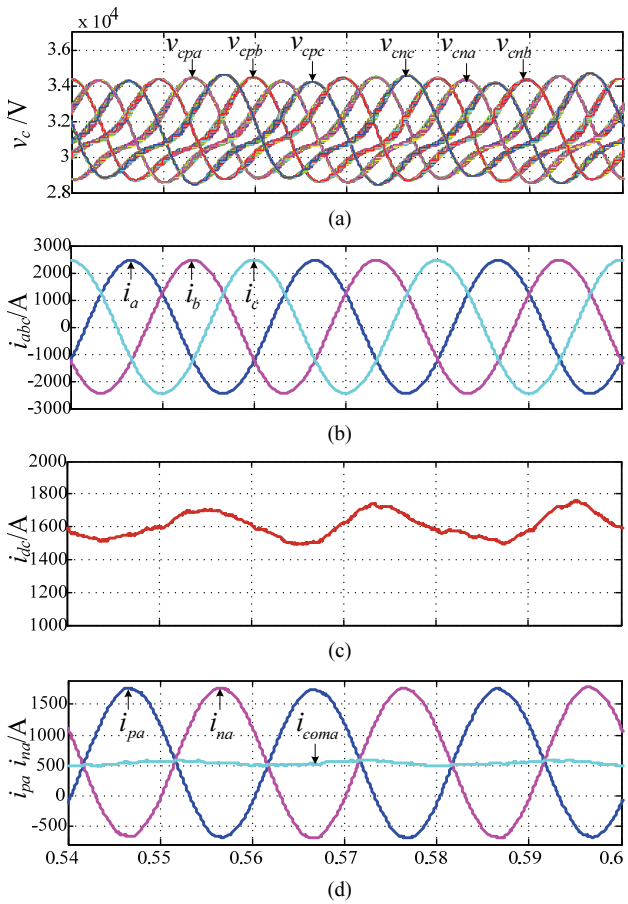

Fig. 7. Steady-state simulation results of MMC1 with conventional control strategy.

control, and MMC2 employs a constant dc voltage control. The simulation parameters of the MMC-HVDC system are shown in Table I, and the arm impedances of MMC2 are identically set to show the negative effect of MMC1 with asymmetric arm impedance on MMC2 in the MMC-HVDC system.

The steady-state simulation results of MMC1 and MMC2 using the conventional control strategy are shown in Figs. 7 and 8, respectively. The operating performance of MMC2 is affected by that of MMC1. Capacitor voltage imbalance among the arms occurs in the two converters. The Fourier analysis results of the ac side and dc side are shown in Table II. The ac side contains dc and double-frequency components, and a fundamental frequency oscillation occurs in the dc side of the two converters.

The steady-state simulation results of MMC1 and MMC2

TABLE I
SIMULATION PARAMETERS OF THE SYSTEM

Parameter	Value
Rated active power	1000MW
DC-link voltage	640kV
AC rated rms voltage	400/333kV
Grid frequency	50Hz
Numbers of SMs per arm	20
SM capacitance	0.5mF(30kJ/MVA)
L_{pa} of MMC1	52.5mH(0.16pu)
L_{na} of MMC1	47.5mH(0.14pu)
L_{pb} of MMC1	50mH(0.15pu)
L_{nb} of MMC1	47.5mH(0.14pu)
L_{pc} of MMC1	47.5mH(0.14pu)
L_{nc} of MMC1	52.5mH(0.16pu)
R_{pa} of MMC1	1.115Ω(0.0105pu)
R_{na} of MMC1	1.045Ω(0.0095pu)
R_{pb} of MMC1	1.1Ω(0.01pu)
R_{nb} of MMC1	1.045Ω(0.0095pu)
R_{pc} of MMC1	1.045Ω(0.0095pu)
R_{nc} of MMC1	1.115Ω(0.0105pu)
Arm inductance of MMC2	50mH(0.15pu)
Arm resistance of MMC2	1.1Ω(0.01pu)
Transformer inductance	50mH(0.15pu)
Sampling frequency	10kHz
DC line length	60km
DC line inductance	0.2285mH/km
DC line resistance	0.0142Ω/km
DC line capacitance	0.1983uF/km

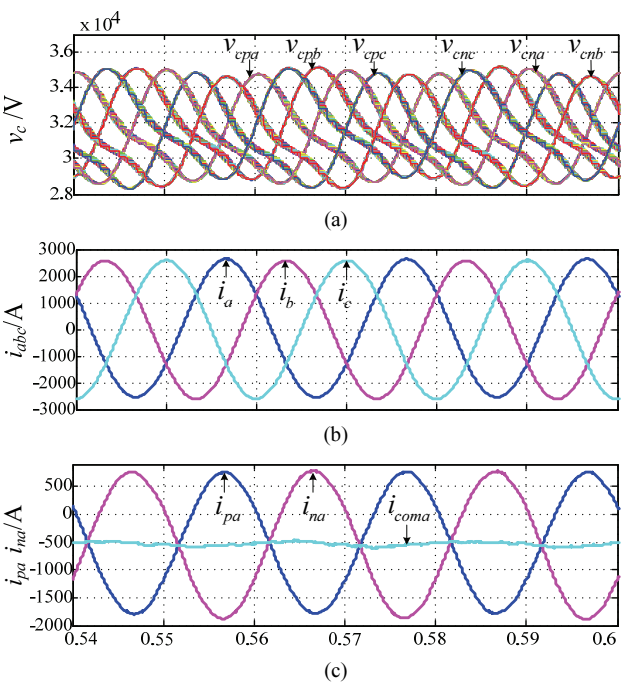

Fig. 8. Steady-state simulation results of MMC2 with conventional control strategy.

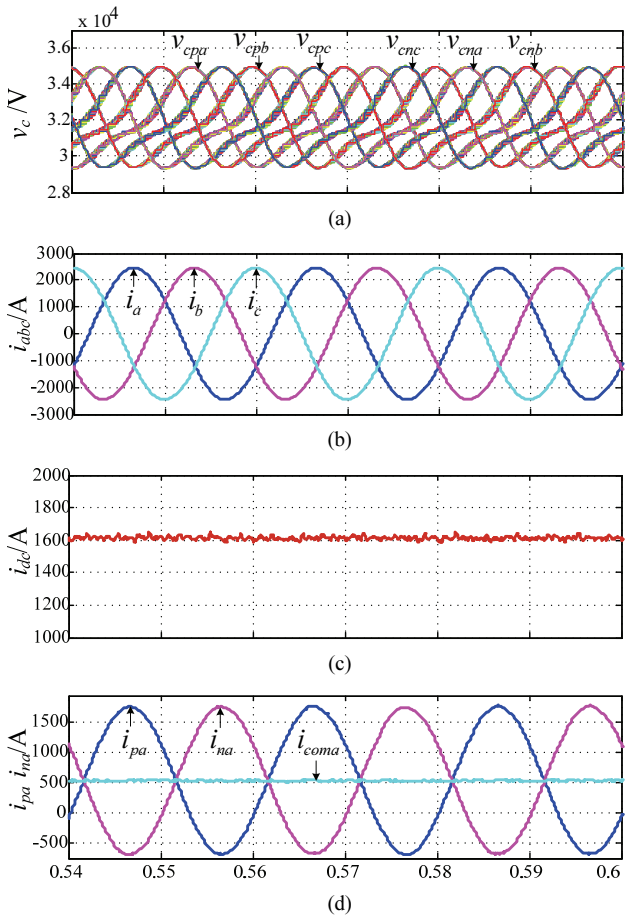

Fig. 9. Steady-state simulation results of MMC1 with enhanced control strategy.

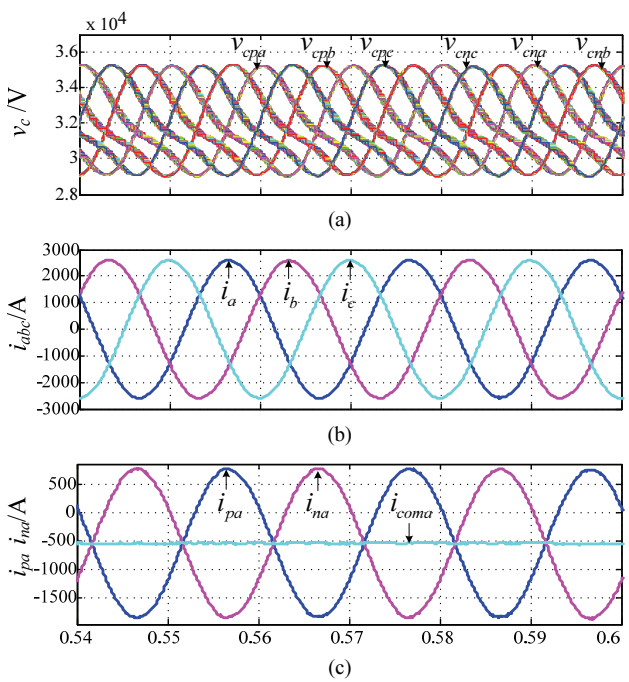

Fig. 10. Steady-state simulation results of MMC2 with enhanced control strategy.

TABLE II
FOURIER ANALYSIS RESULTS OF SIMULATION WAVEFORMS

	i_a		i_{dc}	
	0Hz	100Hz	50Hz	100Hz
Fig. 7	0.68%	0.34%	6.9%	0.58%
Fig. 8	0.71%	0.56%	6.9%	0.58%
Fig. 9	0.03%	0.03%	0.04%	0.03%
Fig. 10	0.03%	0.03%	0.04%	0.03%

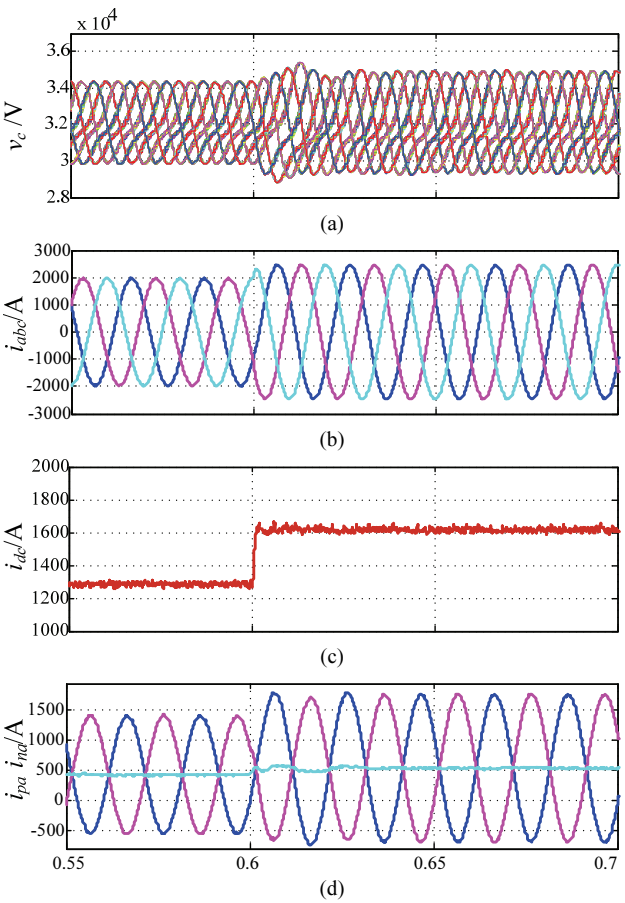

Fig. 11. Dynamic simulation results of MMC1 with enhanced control strategy.

adopting the enhanced control strategy are shown in Figs. 9 and 10, respectively. The capacitor voltages are well-balanced among the arms in the two converters. The Fourier analysis results of the ac and dc sides are shown in Table II. When the enhanced control strategy is adopted, the dc component of the ac side of MMC1 is reduced from 0.68% to 0.03%, the double frequency component of the ac side of MMC1 is reduced from 0.34% to 0.03%, the fundamental frequency oscillation of the dc side is reduced from 6.9% to 0.04%, the dc component of the ac side of MMC2 is reduced from 0.71% to 0.03%, and the double frequency component of the ac side of MMC2 is reduced from 0.56% to 0.03%. The simulation results verify the effectiveness of the proposed enhanced control strategy.

Figs. 11 and 12 present the dynamic results of MMC1 and

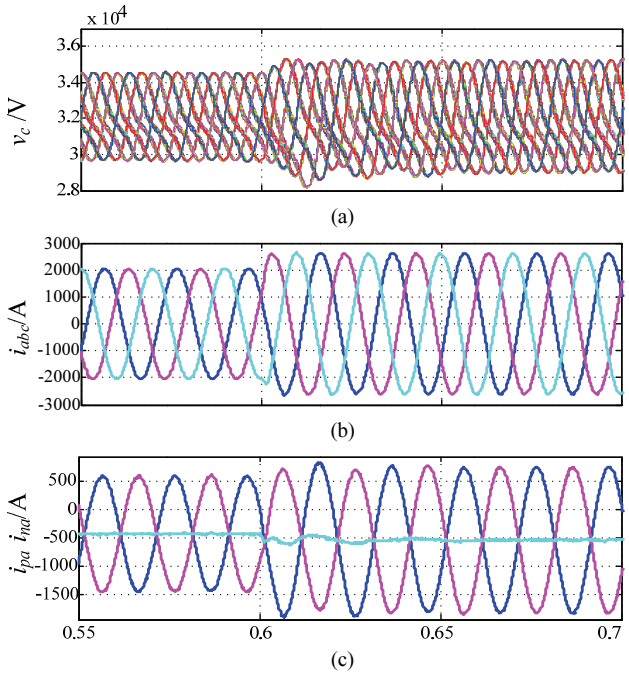

Fig. 12. Dynamic simulation results of MMC2 with enhanced control strategy.

MMC2 using the enhanced control strategy. The active power is increased from 800 MW to 1000 MW at t = 0.6 s. The ac side, dc side, and capacitor voltages in the two converters can rapidly enter the new steady state, and the ac side control, dc side control, and capacitor voltage balance control among the arms are decoupled from one another. This result verifies the good dynamic performance of the enhanced control strategy.

V. Experimental Verification

A downscaled three-phase MMC prototype is built in the laboratory to verify the effectiveness of the proposed enhanced control strategy. The photograph of the prototype is shown in Fig. 13, and the main circuit parameters are listed in Table III. In the experiment, the MMC operates in a fixed active power control mode. The dc bus of the converter is connected to a dc programmable power supply, and the ac side of the converter is connected to the ac power grid through the transformer. In addition, four additional SMs in the bypass state are connected in series to the upper arm of phase a, upper arm of phase b, and lower arm of phase c to simulate the asymmetric arm resistance condition because the arm resistance of the prototype is difficult to be accurately quantified.

The steady-state experimental results of the MMC with asymmetric arm impedance adopting the conventional control strategy are shown in Fig. 14. The capacitor voltage imbalance occurs in the upper and lower arms of phase a. The data stored in the controller are transferred to the host computer (LabVIEW) through the Ethernet and are imported in MATLAB for Fourier analysis. The analysis results are shown in Table IV. The ac side contains the dc and double frequency

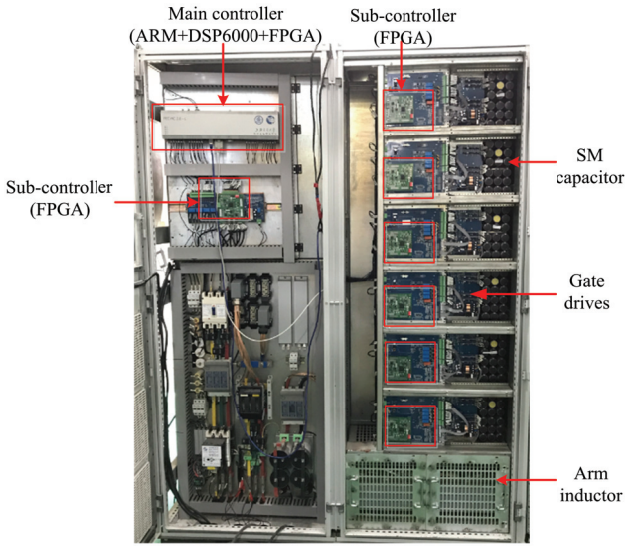

Fig. 13. Photograph of the three-phase MMC prototype.

TABLE III
Downscaled Prototype Parameters

Parameter	Value
Rated active power	4.5kW
DC-link voltage	300V
AC rated rms voltage	380/120V
Grid frequency	50Hz
Numbers of SMs per arm	6
SM capacitance	9mF
L_{pa}	3.3mH
L_{na}	2.8mH
L_{pb}	3.1mH
L_{nb}	2.8mH
L_{pc}	2.9mH
L_{nc}	3.1mH
Sampling frequency	6kHz

components, and a fundamental frequency oscillation occurs in the dc side.

The steady-state experimental results of the MMC with asymmetric arm impedance using the enhanced control strategy are shown in Fig. 15. The capacitor voltages are well-balanced in the upper and lower arms of phase a. The Fourier analysis results of the current waveforms are shown in Table IV. When the enhanced control strategy is adopted, the dc component of the ac side is reduced from 0.92% to 0.03%, the double frequency component of the ac side is reduced from 0.61% to 0.04%, and the fundamental frequency oscillation of the dc side is reduced from 8.5% to 0.06%. Hence, the effectiveness

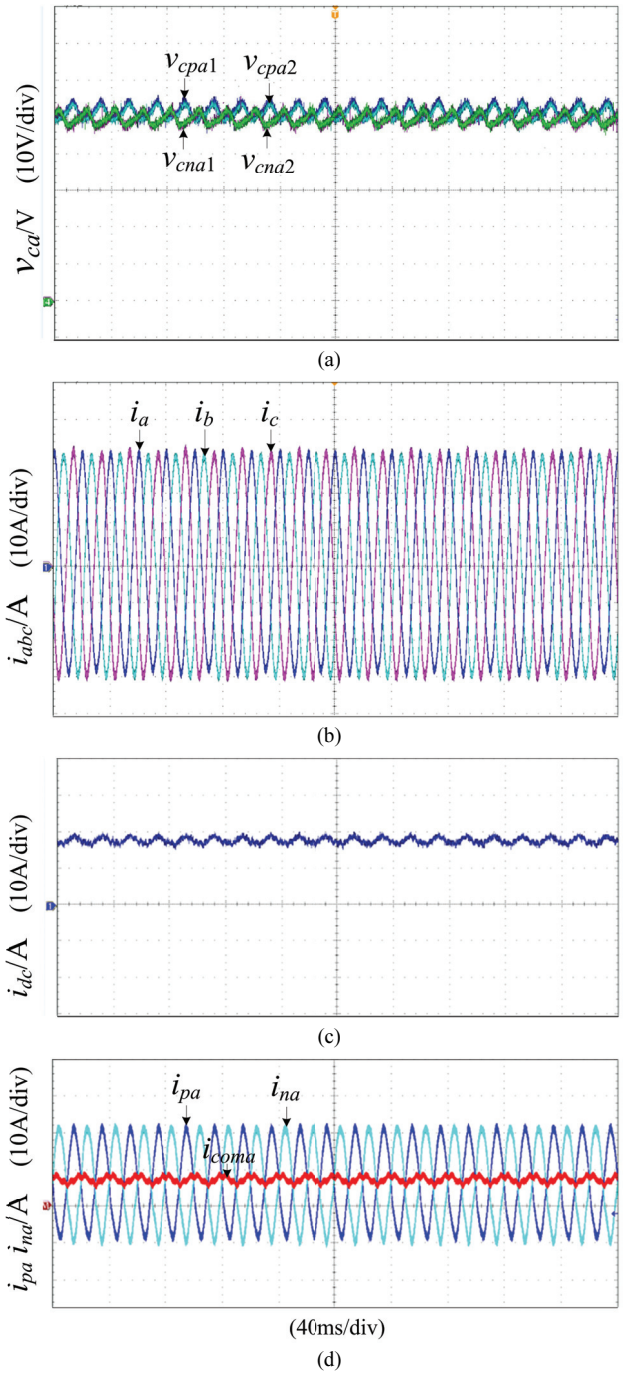

Fig. 14. Steady-state experimental waveforms of the MMC with conventional control strategy.

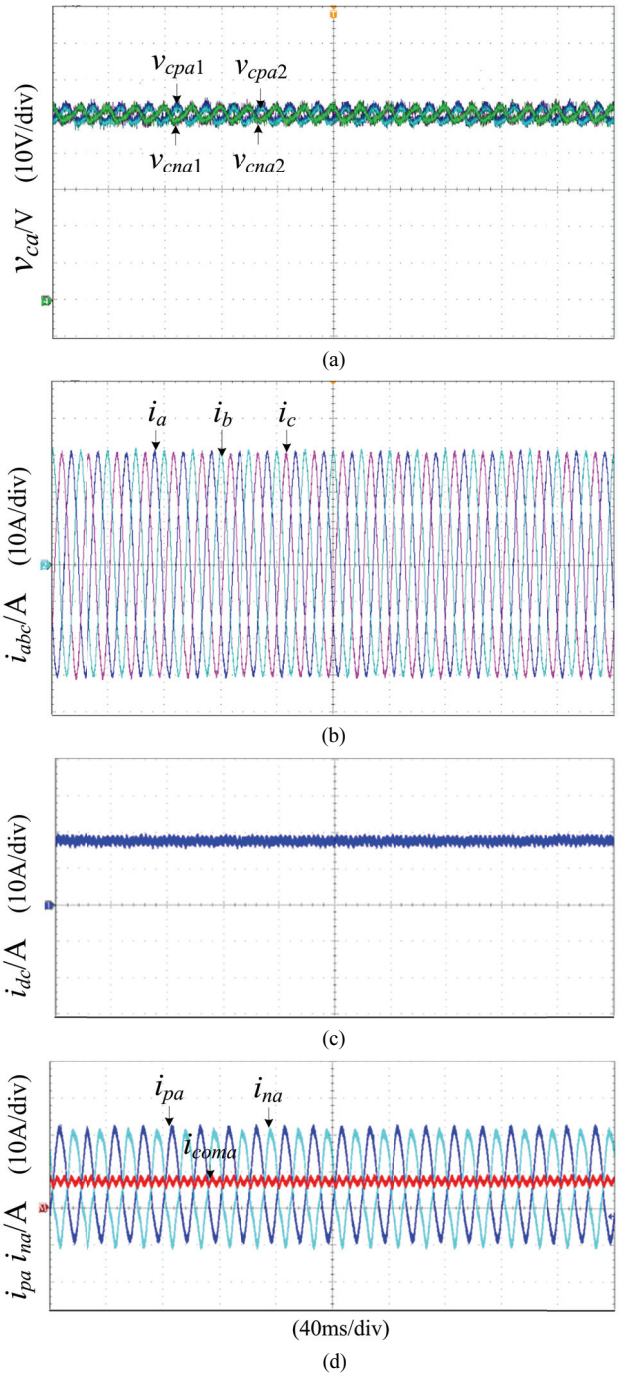

Fig. 15. Steady-state experimental waveforms of the MMC with enhanced control strategy.

of the proposed enhanced control strategy is confirmed by the experimental results.

TABLE IV
FOURIER ANALYSIS RESULTS OF EXPERIMENTAL WAVEFORMS

	i_a		i_{dc}	
	0 Hz	100 Hz	50 Hz	100 Hz
Fig. 14	0.92%	0.61%	8.5%	0.6%
Fig. 15	0.03%	0.04%	0.06%	0.03%

Fig. 16 presents the dynamic results of the MMC with asymmetric arm impedance under the enhanced control strategy. The active power is changed from 3.6 kW to 4.5 kW at t_0; the ac side, dc side, and capacitor voltages can rapidly enter the new steady state; and the ac side control, dc side control, and capacitor voltage balance control among the arms are decoupled from one another. This result shows the good dynamic performance of the proposed enhanced control strategy.

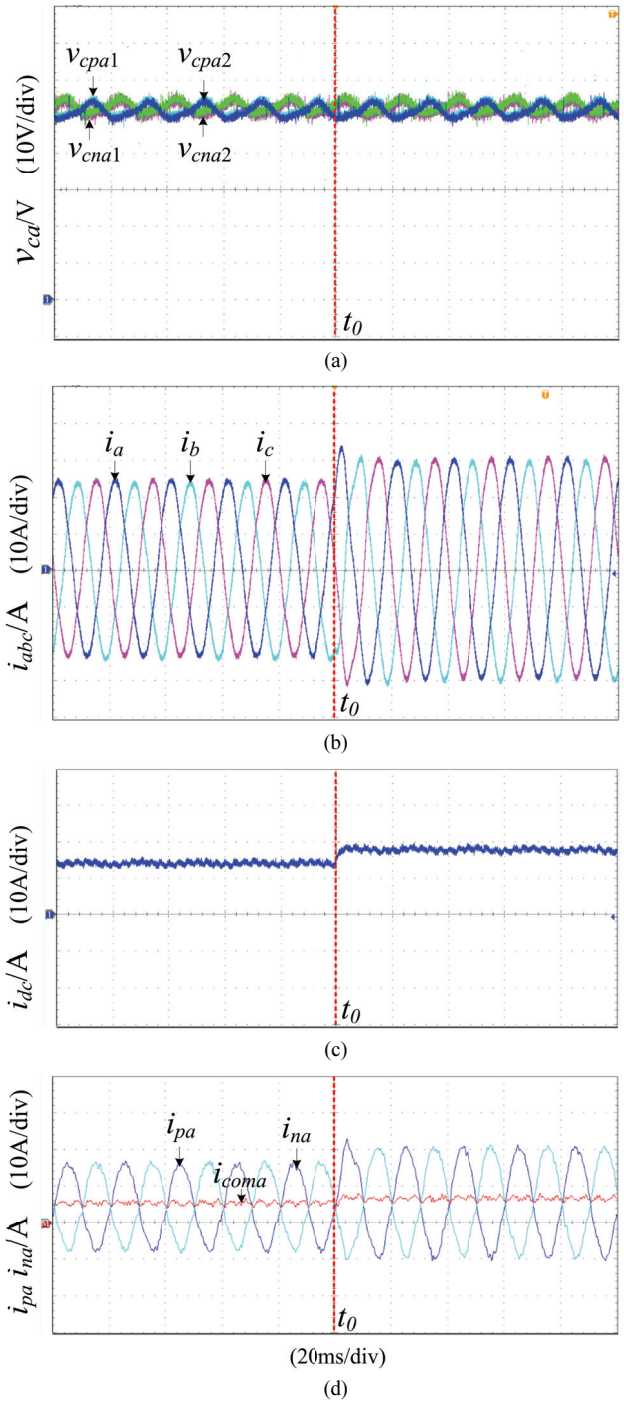

Fig. 16. Dynamic experimental waveforms of the MMC with enhanced control strategy.

VI. Conclusions

In this study, a mathematical model of an MMC with asymmetric arm impedance is established. The causes of the abnormal phenomena are analyzed on the basis of this model. An enhanced control strategy is proposed to eliminate the fundamental frequency oscillations in the dc side and the dc and double frequency components in the ac side current. Such strategy is also used to balance the capacitor voltages among the arms with high efficiency. With the proposed enhanced control strategy, the MMC with asymmetric arm impedance for HVDC applications can achieve superior dynamic performance. The simulation and experimental results verify the accuracy of the theoretical analysis and the effectiveness of the proposed enhanced control strategy.

Appendix

The arm reference voltages can be expressed as

$$\begin{cases} u_{pjref} = -u_{jref} + u_{dcref} + u_{cirjref} \\ u_{njref} = u_{jref} + u_{dcref} + u_{cirjref} \end{cases} \quad \text{(A1)}$$

where u_{jref}, u_{dcref}, and $u_{cirjref}$, (j = a, b, c) are the reference voltages generated by the ac side controller, dc side controller, and circulating current controller, respectively. u_{pjref} and u_{njref} are the reference voltages of the upper and lower arms in phase-j, respectively.

Hence, Equation (A1) can be rewritten as a matrix form, which is expressed as

$$\begin{bmatrix} u_{paref} \\ u_{naref} \\ u_{pbref} \\ u_{nbref} \\ u_{pcref} \\ u_{ncref} \end{bmatrix} = \underbrace{\begin{bmatrix} -1 & 0 & 0 & 1 & 1 & 0 & 0 \\ 1 & 0 & 0 & 1 & 1 & 0 & 0 \\ 0 & -1 & 0 & 1 & 0 & 1 & 0 \\ 0 & 1 & 0 & 1 & 0 & 1 & 0 \\ 0 & 0 & -1 & 1 & 0 & 0 & 1 \\ 0 & 0 & 1 & 1 & 0 & 0 & 1 \end{bmatrix}}_{A} \begin{bmatrix} u_{aref} \\ u_{bref} \\ u_{cref} \\ u_{dcref} \\ u_{ciraref} \\ u_{cirbref} \\ u_{circref} \end{bmatrix} \quad \text{(A2)}$$

Acknowledgment

This work was supported by the National Key Research and Development Program of China under Grant 2016YFB0900901.

References

[1] M. A. Perez, S. Bernet, J. Rodríguez, S. Kouro, and R. Lizana, "Circuit topologies, modeling, control schemes, and applications of modular multilevel converters," *IEEE Trans. Power Electron.*, Vol. 30, No. 1, pp. 4-17, Jan. 2015.

[2] S. Debnath, J. Qin, B. Bahrani, M. Saeedifard, and P. Barbosa, "Operation, control, and applications of the modular multilevel converter: A review," *IEEE Trans. Power Electron.*, Vol. 30, No. 1, pp. 37-53, Jan. 2015.

[3] A. Dekka, B. Wu, R. L. Fuentes, M. Perez, and N. R. Zargari, "Evolution of topologies, modeling, control schemes, and applications of modular multilevel converters," *IEEE J. Emerg. Sel. Topics Power Electron.*, Vol. 5, No. 4, pp. 1631-1656, Dec. 2017.

[4] A. Nami, J. Liang, F. Dijkhuizen, and G. Demetriades, "Modular multilevel converters for HVDC applications: Review on converter cells and functionalities," *IEEE Trans. Power Electron.*, Vol. 30, No. 1, pp. 18-36, Jan. 2015.

[5] R. Marquardt, "Modular multilevel converter: Impact on future applications and semiconductors," *Power Electronic Components and their Applications 2017; 7. ETG-Symposium*, pp. 1-10, Apr. 2017.

[6] J. Kolb, F. Kammerer, M. Gommeringer, and M. Braun, "Cascaded control system of the modular multilevel converter for feeding variable-speed drives," *IEEE Trans. Power Electron.*, Vol. 30, No. 1, pp. 349-357, Jan. 2015.

[7] A. Lesnicar and R. Marquardt, "An innovative modular multilevel converter topology suitable for a wide power range," *IEEE Power Tech Conference*, pp. 23-26, 2003.

[8] H. M. Pirouz, M. T. Bina, and K. Kanzi, "A new approach to the modulation and DC-link balancing strategy of modular multilevel AC/AC converters," *2005 International Conference on Power Electronics and Drives Systems*, pp. 1503-1507, 2005.

[9] L. Harnefors, A. Antonopoulos, S. Norrga, L. Angquist, and H. P. Nee, "Dynamic analysis of modular multilevel converters," *IEEE Trans. Ind. Electron.*, Vol. 60, No. 7, pp. 2526-2537, Apr. 2013.

[10] D. C. Ludois and G. Venkataramanan, "Simplified terminal behavioral model for a modular multilevel converter," *IEEE Trans. Power Electron.*, Vol. 29, No. 4, pp. 1622-1631, Apr. 2014.

[11] R. Lizana, M. Perez, S. Bernet, J. Espinoza, and J. Rodríguez, "Control of arm capacitor voltages in modular multilevel converters," *IEEE Trans. Power Electron.*, Vol. 31, No. 2, pp. 1774-1784, Feb. 2016.

[12] G. Bergna, J. A. Suul, and S. D'Arco, "State-space modelling of modular multilevel converters for constant variables in steady-state," *IEEE 17th Workshop on Control and Modeling for Power Electronics*, pp. 1-9, 2016.

[13] A. Jamshidifar and D. Jovcic, "Small-signal dynamic dq model of modular multilevel converter for system studies," *IEEE Trans. Power Del.*, Vol. 31, No. 1, pp. 191-199, Feb. 2016.

[14] G. Bergna-Diaz, Freytes, X. Guillaud, J. A. Suul, S. D'Arco and J. A. Suul, "Generalized voltage-based state-space modeling of modular multilevel converters with constant equilibrium in steady state," *IEEE J. Emerg. Sel. Topics Power Electron.*, Vol. 6 , No. 2, pp. 707-725, Jun. 2018.

[15] M. Hagiwara and H. Akagi, "Control and analysis of modular multilevel cascade converter based on double-star chopper-cells (MMCC–DSCC)," *IEEE Trans. Power Electron*., Vol. 26, No. 6, pp. 1649-1658, Jun. 2011.

[16] X. She and A. Huang, "Circulating current control of double-star chopper-cell modular multilevel converter for HVDC system," in *Proceeding of IECON*, pp. 1234-1239, Oct. 2012.

[17] M. Zhang, L. Huang, W. Yao, and Z. Lu, "Circulating harmonic current elimination of a CPS-PWM-based modular multilevel converter with a plug-in repetitive controller," *IEEE Trans. Power Electron.*, Vol. 29, No. 4, pp. 2083-2097, Apr. 2014.

[18] A. Antonopoulos, L. Angquist, and H. P. Nee, "On dynamics and voltage control of the Modular Multilevel Converter," *13th Power Electronics and Applications Conference*, pp. 1-10, Oct. 2009.

[19] J. Freytes, G. Bergna, J. A. Suul, S. D'Arco, H. Saad, and X. Guillaud, "State-space modelling with steady-state time invariant representation of energy based controllers for modular multilevel converters," *2017 IEEE Manchester PowerTech*, pp. 1-7, 2017.

[20] G. Bergna-Diaz, J. A. Suul, and S. D'Arco, "Energy- based state space representation of modular multilevel converters with a constant equilibrium point in steady-state operation," *IEEE Trans. Power Electron.*, Vol. 33, No. 6, pp. 4832-4851, Jun. 2018.

[21] X. Shi, Z. Wang, B. Liu, Y. Li, L. M. Tolbert, and F. Wang, "Steady-state modeling of modular multilevel converter under unbalanced grid conditions," *IEEE Trans. Power Electron.*, Vol. 32, No. 9, pp. 7306-7324, Sep. 2017.

[22] J. W. Moon, J. W. Park, D. W. Kang, and J. M. Kim, "A control method of HVDC-modular multilevel converter based on arm current under the unbalanced voltage condition," *IEEE Trans. Power Del.*, Vol. 30, No. 2, pp. 529-536, Aug. 2015.

[23] Q. Tu, Z. Xu, Y. Chang, and L. Guan, "Suppressing DC voltage ripples of MMC-HVDC under unbalanced grid conditions," *IEEE Trans. Power Del.*, Vol. 27, No. 3, pp. 1332-1338, Jul. 2012.

[24] X. Shi, Z. Wang, B. Liu, Y. Li, L. M. Tolbert, and F. Wang, "Characteristic investigation and control of modular multilevel converter based HVDC system under single-line-to-ground fault conditions," *IEEE Trans. Power Electron.*, Vol. 30, No. 1, pp. 408-421, Jan. 2015.

[25] G. Bergna, J. A. Suul, E. Berne, J. C. Vannier, and M. Molinas, "MMC circulating current reference calculation in ABC frame by means of lagrange multipliers for ensuring constant DC power under unbalanced grid conditions," *European Conference on Power Electronics and Applications*, pp. 1-10, 2014.

[26] Y. Zhou, D. Jiang, J. Guo, P. Hu, and Y. Liang, "Analysis and control of modular multilevel converters under unbalanced conditions," *IEEE Trans. Power Electron.*, Vol. 28, No. 4, pp. 1986-1995, Oct. 2013.

[27] R. Zeng, L. Xu, L. Yao, and S. J. Finney, "Analysis and Control of Modular Multilevel Converters under Asymmetric Arm Impedance Conditions," *IEEE Trans. Ind. Electron.*, Vol.63, No.1, pp. 71-81, Jan. 2016.

[28] A. R. Lopez-Nunez, J. D. Mina, J. Aguayo, and G. Calderon, "Proportional integral resonant controller for current harmonics mitigation in a wind energy conversion system," *International power electronics congress-CIEP*, pp. 232- 237, 2016.

[29] A. Ferreira, O. Gomis-Bellmunt, and M. Teixido, "Modular multilevel converter modeling and controllers design," in *Proc. ECCE Europe*, pp. 1-10, 2014.

[30] L. Harnefors and H.-P. Nee, "Model-based current control of ac machines using the internal model control method," *IEEE Trans. Ind. Appl.*, Vol. 34, No. 1, pp. 133-141, Jan. 1998.

[31] M. Hagiwara and H. Akagi, "Control and experiment of pulsewidth-modulated modular multilevel converters," *IEEE Trans. Power Electron*., Vol. 24, No. 7, pp. 1737-1746, Jul. 2009.

[32] F. Deng and Z. Chen, "A control method for voltage balancing in modular multilevel converters," *IEEE Trans. Power Electron*., Vol. 29, No. 1, pp. 66-76, Jan. 2014.

[33] Q. Tu, Z. Xu, and L. Xu, "Reduced switching-frequency modulation and circulating current suppression for modular multilevel converters," *IEEE Trans. Power Del.*, Vol. 26, No. 3, pp. 2009-2017, Apr. 2011.

[34] Y. Li, E. A. Jones, and F. Wang, "The impact of voltage-balancing control on switching frequency of the modular multilevel converter," *IEEE Trans. Power Electron*., Vol. 31, No. 4, pp. 2829-2839, Apr. 2016.

Peng Dong was born in Yantai, China, in 1990. He received his B.Eng. degree in Electronical Engineering from China University of Mining and Technology, Jiangsu, China, in 2013. He is currently working toward his Ph.D. degree in Electrical Engineering at Shanghai Jiao Tong University, Shanghai, China. His current interests include the modeling and control of MMCs and high-power electronics.

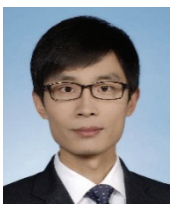

Jing Lyu was born in Xuzhou, China, in 1985. He received his B.Eng. degree in Electrical Engineering and Automation from China University of Mining and Technology, Jiangsu, China, in 2009. He received his M.Eng. and Ph.D. degrees in Electrical Engineering from Shanghai Jiao Tong University, Shanghai, China, in 2011 and 2016, respectively. He served as a Research Fellow at the Department of Engineering Cybernetics, Norwegian University of Science and Technology, Trondheim, Norway, from 2016 to 2017. He is currently an Assistant Professor at the Department of Electrical Engineering, Shanghai Jiao Tong University. His current research interests include the dynamic stability of MMC-based HVDC connected wind farms/PV plants, modeling and control of MMCs, wind power converters, and impedance modeling.

Xu Cai was born in Xuzhou, China, in 1964. He received his B.Eng. degree from Southeast University, Nanjing, China, in 1983. He received his M.Sc. and Ph.D. degrees from China University of Mining and Technology, Jiangsu, China, in 1988 and 2000, respectively. He served as an Associate Professor at the Department of Electrical Engineering, China University of Mining and Technology from 1989 to 2001. He worked as a Professor in Shanghai Jiao Tong University in 2002, Director of the Wind Power Research Center of Shanghai Jiao Tong University in 2008, and Vice Director of the State Energy Smart Grid R&D Center (Shanghai) from 2010 to 2013. His special fields of interest are power electronics and renewable energy exploitation and utilization, which include wind power converters, wind turbine control systems, large power battery storage systems, and clustering of wind farms and their control system and grid integration.